

High-fidelity Pseudo-labels for Boosting Weakly-Supervised Segmentation

Arvi Jonnarth* Yushan Zhang Michael Felsberg†
 Department of Electrical Engineering, Linköping University, Sweden
 {arvi.jonnarth, yushan.zhang, michael.felsberg}@liu.se

Abstract

The task of image-level weakly-supervised semantic segmentation (WSSS) has gained popularity in recent years, as it reduces the vast data annotation cost for training segmentation models. The typical approach for WSSS involves training an image classification network using global average pooling (GAP) on convolutional feature maps. This enables the estimation of object locations based on class activation maps (CAMs), which identify the importance of image regions. The CAMs are then used to generate pseudo-labels, in the form of segmentation masks, to supervise a segmentation model in the absence of pixel-level ground truth. In case of the SEAM baseline, a previous work proposed to improve CAM learning in two ways: (1) Importance sampling, which is a substitute for GAP, and (2) the feature similarity loss, which utilizes a heuristic that object contours almost exclusively align with color edges in images. In this work, we propose a different probabilistic interpretation of CAMs for these techniques, rendering the likelihood more appropriate than the multinomial posterior. As a result, we propose an add-on method that can boost essentially any previous WSSS method, improving both the region similarity and contour quality of all implemented state-of-the-art baselines. This is demonstrated on a wide variety of baselines on the PASCAL VOC dataset. Experiments on the MS COCO dataset show that performance gains can also be achieved in a large-scale setting. Our code is available at <https://github.com/arvijj/hfpl>.

1. Introduction

Recent years have witnessed significant advancements in deep learning methods, impacting many computer vision tasks, including semantic segmentation. Automatic image segmentation has proven useful in many applications, including autonomous driving [9], video surveillance [15], and medical image analysis [34]. Although remarkable results have been achieved by fully-supervised segmentation

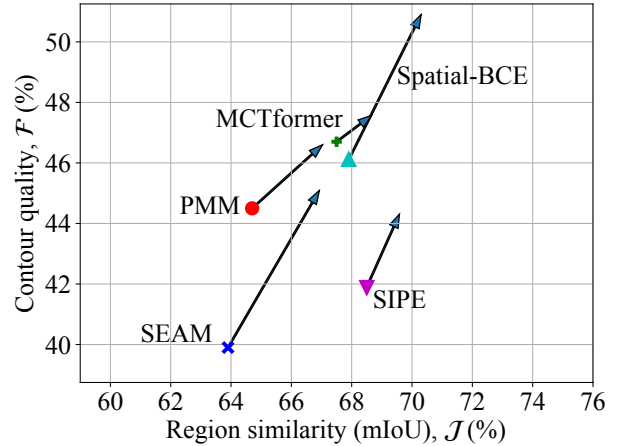


Figure 1: Region similarity (\mathcal{J}) versus contour quality (\mathcal{F}) for different state-of-the-art baselines on the VOC validation set. The arrows represent improvements by our proposed importance sampling loss and feature similarity loss.

frameworks, the utilization of large datasets with pixel-wise annotated images necessitates a significant manual labeling effort, which increases with the dataset size. To address this challenge, weakly-supervised semantic segmentation (WSSS) aims to alleviate the labelling effort by other alternatives, such as image-level labels [46], bounding boxes [10], scribbles [31], and points [4]. Out of all the available options, image-level classification labels are the most cost-effective and can be obtained from various sources, making them the most popular choice for WSSS.

WSSS with image-level supervision aims to produce pseudo-masks for images from classification labels only. For this purpose, class activation maps (CAMs) [55] are exploited in many methods. While this approach has been shown to have a remarkable ability for localization, it does not take the object shape into account. This leads to activation mostly around discriminative regions and overly smooth CAMs, without well-defined prediction contours. This is due to the nature of global average pooling where all the pixels in the image are treated as the same category, which is problematic in the background areas. In the par-

*Affiliation: Husqvarna Group, Huskvarna, Sweden.

†Co-affiliation: University of KwaZulu-Natal, Durban, South Africa.

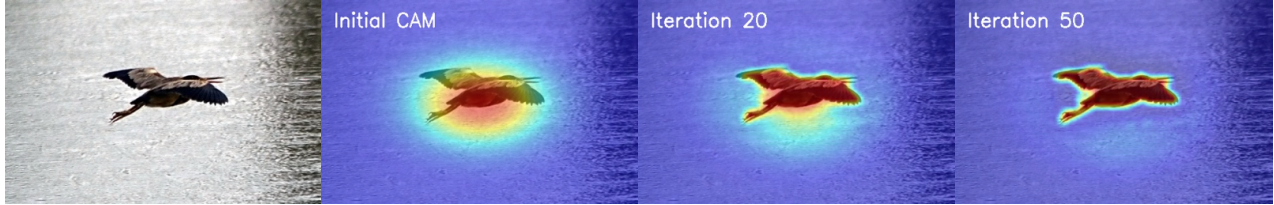


Figure 2: Illustration of how the feature similarity loss can improve an initial CAM.

ticular case of SEAM, two complementary techniques have been proposed to overcome this drawback [19]: (1) The importance sampling loss (ISL), which is adopted to decouple the foreground and background areas; (2) the feature similarity loss (FSL), which is used to improve the contours of the predicted segmentations. Furthermore, FSL improves the sampling distribution of ISL, which is illustrated in Figure 2. The foreground and background are decoupled in this way, and the image-level categories are only assigned to the proper foreground pixels.

Based on the approach using ISL and FSL [19], we propose four contributions. First, we model the likelihood as opposed to the multinomial posterior. This is because the class-wise softmax normalization on the pixel-level does not make sense if two classes can share the space occupied by a single pixel, which is especially true in down-sampled CAMs. If two classes share the same pixel, the activation is not drawn from a single distribution, but from two. Moreover, the normalization is done over each pixel, which destroys the continuous information between adjacent pixels. Second, we generalize ISL and FSL to virtually any WSSS method, based on modeling the likelihood. Due to the setting of various WSSS methods, the multinomial posterior is not always suitable for importance sampling, especially if it is only computed based on the foreground classes, in which case the importance sampling frequency of each pixel will sum to one. This is not a desired behavior since we want the foreground to be sampled more frequently than the background. By moving from posterior to likelihood, this problem is well addressed. Third, the original ISL [19] only samples one pixel per class, which is analogous to global max pooling. We instead sample multiple pixels to simulate global average pooling, which is more powerful, as it allows backpropagation over a larger region. Fourth, we perform exhaustive experiments and boost the performance on no less than five recent methods, which is demonstrated in Figure 1. We evaluate these methods, besides on the common region similarity, also on their contour accuracy.

2. Related work

Types of weak supervision. Full supervision of semantic segmentation requires pixel-wise annotations, which are difficult to acquire and can suffer from inaccuracies. There-

fore, it is of interest to investigate weak supervision that requires less manual labeling. Bounding boxes are a natural substitute for pixel-wise labels, and are exploited in different works [35, 20, 10, 27]. Inspired by interactive image segmentation, scribbles [31, 45] and points [5] have been used to ease the annotation. Image classification labels [55], which are the easiest to acquire, are also the most common.

Pseudo-label generation from image classification labels constitutes a core part of WSSS. Zhou *et al.* [55] introduced class activation maps (CAMs) by revisiting the global average pooling (GAP) layer in classification networks, and showed that they had a remarkable localization ability, despite being trained with only classification labels. However, CAMs usually only activate over small and sparse discriminative regions. Subsequent works aim to overcome this drawback. Kolesnikov *et al.* [21] introduced a global weighted rank pooling to replace GAP, and a constrain-to-boundary loss to learn precise boundaries during training. Wei *et al.* [47] proposed an adversarial erasing approach to mining and expanding object regions continuously. Li *et al.* [29] introduced a self-guidance scheme on CAMs to force them to activate on objects holistically. Huang *et al.* [17] utilized the classical seeded region growing method to expand the discriminative regions to cover the entire objects in an end-to-end fashion. Wei *et al.* [48] utilize dilated convolutions to enlarge the receptive field and to effectively transfer the information from discriminative to non-discriminative regions. Lee *et al.* [25] proposed FickleNet using dropout to stochastically select hidden units, and allow a single network to generate multiple localization maps corresponding to different parts of the objects. Wang *et al.* [46] proposed a self-supervised equivariant attention mechanism (SEAM) by imposing consistency regularization in a siamese network. Wu *et al.* [50] introduced an embedded discriminative attention mechanism to generate class-specific activation maps by exploring the inter-image and intra-image homogeneity. Closely related to our work, Jonnarth and Felsberg [19] performed importance sampling as a substitute for GAP, and introduced an auxiliary feature similarity loss as additional supervision for SEAM [46]. The main differences are: (1) We model the independent likelihoods instead of the multinomial posterior; (2) we generalize ISL and FSL from SEAM to virtually any method;

(3) we introduce multi-pixel sampling to simulate GAP.

Pseudo-label refinement takes the CAMs as input, and outputs refined pseudo-labels without re-training the CAMs. Ahn *et al.* [2] proposed AffinityNet that predicts class-agnostic pixel-level semantic affinity. They further explored inter-pixel relations (IRN) [1], where confident seed areas are identified, and propagated via random walk, to discover the entire object with accurate boundaries. Chen *et al.* [6] explored object boundaries explicitly and used the explored boundaries to constrain the localization map propagation. Lee *et al.* [26] introduced an anti-adversarial technique to manipulate images for increasing its classification score, which allows it to identify more regions on objects.

3. Preliminaries

3.1. The weakly-supervised segmentation task

We consider the image-level weakly-supervised semantic segmentation (WSSS) task. As opposed to the fully supervised case, no pixel-wise annotations are used for training. Given a dataset of images and corresponding image-level labels, we aim to train a model that predicts the semantic class for every pixel in an image. Commonly, this is achieved by first training a multi-label classification network, from which pseudo-labels are generated, commonly based on CAMs. Optionally, a pseudo-label refinement method is applied. Finally, a segmentation model is trained in the fully-supervised setting, where the pseudo-labels are used as ground truth. Our contributions focus on the first stage of generating high-fidelity pseudo-labels.

3.2. Class activation maps

Class activation maps (CAM) of different forms have become a core component in the majority of weakly supervised segmentation methods [7, 8, 46]. Zhou *et al.* [55] introduced the CAM concept, and showed that classification networks that use a global average pooling (GAP) layer possess the ability to localize objects without any supervision on their locations, such as bounding boxes or segmentation masks. In their network architecture, they perform GAP on the feature map $f_k(i, j)$ over the spatial coordinates i and j for each channel k , where $f_k(i, j)$ is the output of the final convolutional layer. They then apply a single fully connected layer, and thus, the class score for class c is

$$S_c = \sum_k w_k^c \sum_{i,j} f_k(i, j) = \sum_{i,j} \sum_k w_k^c f_k(i, j), \quad (1)$$

where w_k^c are the weights of the fully connected layer. The weight w_k^c can be seen as the importance of feature k on class c . Thus, they formulate the CAM as

$$M_c(i, j) = \sum_k w_k^c f_k(i, j), \quad (2)$$

which is the weighted sum over the features, and directly indicates the importance at spatial grid position (i, j) [55].

Since CAMs provide the ability to localize objects using only classification labels, they are a natural choice for weakly supervised segmentation. However, most WSSS methods modify the original CAM, by removing the fully connected layer, and explicitly represent the output of the final convolutional layer as the spatial class score $s_c(i, j)$, with the same number of channels, C , as there are classes [7, 46, 51]. In this case, the CAM M_c is equivalent to s_c . GAP is then applied to s_c to get the image-level class score

$$S_c = \sum_{i,j} s_c(i, j). \quad (3)$$

Furthermore, in WSSS, the CAMs are usually normalized to the range $[0, 1]$ for pseudo-label generation. A common method involves ReLU and max normalization [7, 46, 52]

$$r_c(i, j) = \frac{\text{ReLU}(s_c(i, j))}{\max_{m,n} \text{ReLU}(s_c(m, n))}, \quad (4)$$

where r_c represents the normalized CAM. By interpreting the score s as the log-likelihood, which we explore in Section 4, then r can be viewed as the log-likelihood ratio.

A third option for creating CAMs is to model the multinomial posterior per pixel, prior to global pooling [3, 19]. The normalized CAMs are computed using softmax

$$a_c(i, j) = \frac{e^{s_c(i, j)}}{\sum_{k=1}^C e^{s_k(i, j)}} \cong \Pr(z_c(i, j) = 1|x), \quad (5)$$

where C is the number of classes, $z_c(i, j)$ is the true class label, and is 1 if class c occupies position (i, j) , or 0 otherwise. This is used in the fully-supervised case, as the posterior can be directly supervised using segmentation masks.

3.3. Importance sampling loss

Recently, importance sampling has been proposed as a substitute for global pooling during weakly supervised training [19]. It aims to solve the problem of global max pooling (GMP), which mainly target the most discriminative region of an object. The authors in [19] model the multinomial posterior as in (5), and define a probability mass function over pixel coordinates (i, j) ;

$$p_c(I, J|x) = \Pr(I = i, J = j|x, c) = a_c(i, j)/Z(a_c), \quad (6)$$

where $Z(a_c) = \sum_{m=1}^W \sum_{n=1}^H a_c(m, n)$ is a normalizing constant for an image of width W and height H . A pixel is then drawn from this distribution for each class, and the image-level prediction \tilde{y} is computed as

$$\tilde{y}_c = a_c(\hat{i}, \hat{j}), \quad (\hat{i}, \hat{j}) \sim p_c(I, J|x). \quad (7)$$

Finally, the importance sampling loss (ISL) is the binary cross-entropy loss of the sampled prediction

$$\mathcal{L}_{\text{is}}(y, \tilde{y}) = -\frac{1}{C} \sum_{c=1}^C y_c \log \tilde{y}_c + (1 - y_c) \log(1 - \tilde{y}_c), \quad (8)$$

where y is a vector of the image-level classification labels, and y_c is the label for class c , which is 1 if class c is present anywhere in the image, and 0 otherwise.

3.4. Feature similarity loss

Heuristically, objects are in most cases precisely separated from one another, or the background, by a color edge. Jonnarth and Felsberg [19] encapsulate this prior knowledge into the self-supervised feature similarity loss function

$$\mathcal{L}_{\text{fs}}(a, x) = -\frac{1}{HW} \sum_{i,j=1}^{H \cdot W} w_{ij} g(a_i, a_j) f(\delta(x_i, x_j)), \quad (9)$$

which matches the prediction contours with edges in the image. It is a function of the posterior $a \in [0, 1]^{H \times W \times C}$ in (5), and the RGB image $x \in [0, 1]^{H \times W \times 3}$. (Note that the spatial indexing is different for the sake of clarity, where a single index, *i.e.* i or j , is used for both of the spatial coordinates.) The loss term sums over all *pixel pairs*, and consists of three components. First, a Gaussian spatial weight

$$w_{ij} = \frac{1}{2\pi\sigma^2} \exp\left(-\frac{\|p_i - p_j\|_2^2}{2\sigma^2}\right), \quad (10)$$

where p_i is the two-dimensional position vector for pixel i . This assigns a higher importance to nearby pixel pairs. Very distant pairs are disregarded, as little to no conclusion can be drawn about their semantic affinity, solely based on color information. The second component is a gating function

$$g(a_i, a_j) = \frac{1}{2} \|a_i - a_j\|_2^2, \quad (11)$$

which is the distance between the posteriors of pixels i and j . The final component is a pixel dissimilarity function

$$f(\delta) = \tanh\left(\mu + \log\left(\frac{\delta}{1 - \delta}\right)\right), \quad (12)$$

$$\delta(x_i, x_j) = \frac{\|x_i - x_j\|_1}{3}, \quad (13)$$

which maps two RGB pixel values to a dissimilarity score in $[-1, 1]$. See Figure 3 for an illustration of FSL.

Since a is the only variable dependent on the model parameters, $g(a_i, a_j)$ is the part that is optimized over during training. The weight w_{ij} controls the magnitude of the loss, while f controls the sign. Intuitively, two similar pixels imply $f < 0$ and $\mathcal{L}_{\text{fs}} > 0$. In this case, the loss is minimized when g is minimized, *i.e.* when the predictions are the same.

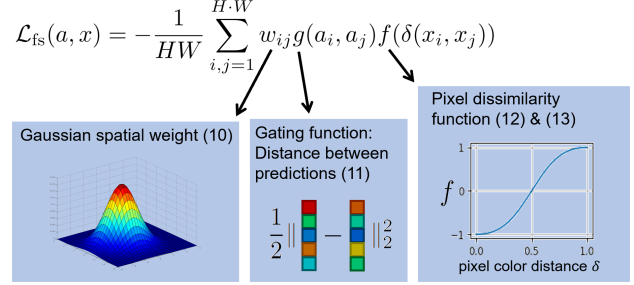


Figure 3: Illustration of the feature similarity loss (FSL).

On the contrary, for two dissimilar pixels, we get $\mathcal{L}_{\text{fs}} < 0$, and the loss is minimized when g is maximized, *i.e.* when the predictions are far apart. However, if the predictions are equal to begin with, then $\nabla \mathcal{L}_{\text{fs}} = 0$, allowing consistent predictions over heterogeneous image regions. This is important for multi-textured objects.

\mathcal{L}_{fs} contains two parameters, the size σ of the spatial weight, and the bias μ of the pixel dissimilarity function. These are trained jointly with the network parameters [19].

4. Likelihood modeling for ISL and FSL

Since the importance sampling loss and feature similarity loss were originally applied when modeling the multinomial posterior [19], they cannot be directly applied to stronger baselines than SEAM [46], since most methods model the likelihood, and use GAP according to (3). We found in our initial experiments that enforcing a posterior estimation with the use of softmax in (5) resulted in performance degradation for other baselines. A likely explanation is that the explicit assumption of mutual exclusivity of classes on the pixel level affects the characteristics of the learned CAMs, and can thus affect optimal hyperparameter values. For example, Jonnarth and Felsberg [19] found it necessary to heavily modify the background parameter α for AffinityNet [2] label generation, since the CAM characteristics had changed. Similarly, optimal hyperparameter values inherent to other baselines could also be affected.

Moreover, the mutual exclusivity assumption is not only problematic due to the fact that several classes can share the space of an image pixel. It becomes entirely void due to the fact that CAMs are usually computed in a lower resolution compared to the original input images, due to the use of a fixed input size and downsampling layers in the network architecture. This means that the assumption is not made on the pixel-level, but in fact, within a small region defined by the final downsampling scale factor. Additionally, identical features can be shared between classes, *e.g.* a wheel on a car, bus or trailer, in which case the evidence is shared over a large image region, independent of pixel resolution.

We argue that ISL and FSL would benefit from relaxing

the mutual exclusivity assumption. Instead of looking at the multinomial, we consider the C -fold binomial problem, which constitutes modeling C binary posteriors. However, the prior is constant and difficult to estimate. Therefore, we, as most WSSS approaches using GAP, go for the likelihood instead. Thus, we aim to adapt ISL and FSL to be compatible with likelihood modeling. A further goal is that ISL and FSL can be seamlessly implemented as add-on methods to any previous or future method, without any major modifications to the underlying baseline.

4.1. Likelihood-based importance sampling loss

A natural approach is to model the pixel-wise likelihood using the sigmoid function, where the likelihood is given by

$$l_c(i, j) = \frac{e^{s_c(i, j)}}{1 + e^{s_c(i, j)}} \cong \Pr(x|z_c(i, j)). \quad (14)$$

The sampling distribution is attained in a similar manner as for the multinomial posterior case, namely

$$p_c(I, J|x) = l_c(i, j)/Z(l_c). \quad (15)$$

We sample the likelihood $\tilde{l}_c = l_c(\hat{i}, \hat{j})$, where $(\hat{i}, \hat{j}) \sim p_c(I, J|x)$, and the final loss is thus computed as $\mathcal{L}_{\text{is}}(y, \tilde{l})$.

Moreover, importance sampling has been shown to be superior to GMP [19]. However, Zhou *et al.* [55] found that while GMP achieves similar classification performance as GAP, GAP outperforms GMP for localization. Thus, we define the final classification loss as a convex combination of the importance sampling loss and binary cross-entropy loss, \mathcal{L}_{ce} , based on GAP, similarly to how the original authors used GMP. Our combined classification loss is

$$\mathcal{L}_{\text{cls}} = (1 - \lambda)\mathcal{L}_{\text{ce}} + \lambda\mathcal{L}_{\text{is}}, \quad (16)$$

$$\mathcal{L}_{\text{ce}} = -\frac{1}{C} \sum_{c=1}^C y_c \log L_c + (1 - y_c) \log(1 - L_c), \quad (17)$$

where $L_c = \exp(S_c)/(1 + \exp(S_c))$ is the image-level GAP likelihood estimate based on S_c in (3).

Finally, to improve stability, we propose to sample multiple pixels per class, and average their loss contributions. We write the multi-sample importance sampling loss as

$$\mathcal{L}_{\text{is}}^N = \frac{1}{N} \sum_{n=1}^N \mathcal{L}_{\text{is}}(y, \tilde{l}^{(n)}), \quad (18)$$

where N is the number of samples drawn per class, and $\tilde{l}^{(n)}$ for $n = 1, \dots, N$ are prediction vectors of length C , containing independently drawn samples. Figure 4 illustrates the difference between GMP, GAP, and multi-sample ISL.

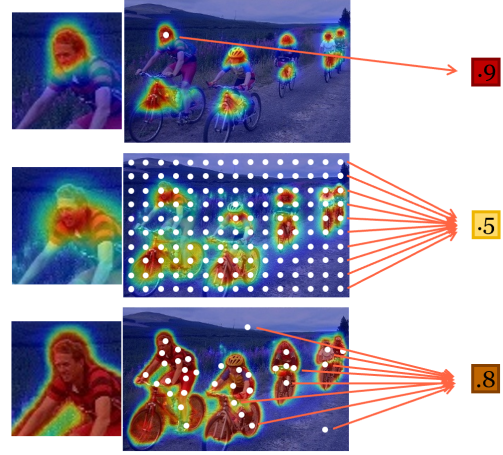


Figure 4: Illustration of global pooling methods. Top to bottom; max pooling, average pooling, importance sampling.

4.2. Likelihood-based feature similarity loss

As for ISL, the assumption made when modeling the multinomial posterior, *i.e.* that classes are mutually exclusive within a small region, also affects the feature similarity loss. For dissimilar pixels, not only are the predictions pushed apart between the pixels, the predictions between classes are also pushed apart. The prediction will tend towards a one-hot vector [19]. Based on the argument in Section 4, *i.e.* that multiple classes can occupy the same pixel, we argue that classes should be handled independently when reasoning about their contours. In fact, we believe that this reasoning is even more important at class borders, as two classes are likely to occupy the same pixel.

Thus, we adapt FSL for likelihood modeling according to (14), where the classes are considered independently, in the absence of softmax. We consider three different inputs to the gating function: The scores s , the likelihood l , and the log-likelihood ratio r . A closer look at the gradients reveals that, when using the scores s directly,

$$\frac{\partial g(s_i, s_j)}{\partial s_{i,c}} = s_{i,c} - s_{j,c}. \quad (19)$$

The gradient is proportional to the score difference. For dissimilar pixels, g is maximized, which leads to divergence, as the gradients increase indefinitely. The gradient is bounded for the likelihood l , we get

$$\left| \frac{\partial g(l_i, l_j)}{\partial s_{i,c}} \right| = \left| (l_{i,c} - l_{j,c}) \frac{e^{s_{i,c}}}{(1 + e^{s_{i,c}})^2} \right| \quad (20)$$

$$\leq e^{s_{i,c}} / (1 + e^{s_{i,c}})^2 \leq 1/e^{s_{i,c}}. \quad (21)$$

The same is true for r . Assuming $s_{i,c} \geq 0$, we get

$$\left| \frac{\partial g(r_i, r_j)}{\partial s_{i,c}} \right| = \left| (r_{i,c} - r_{j,c}) \frac{1}{\max_m(s_{m,c})} \right| \quad (22)$$

$$\leq 1/\max_m(s_{m,c}). \quad (23)$$

Since the gradients are bounded for l and r , the scores do not diverge out of control whenever the prediction difference is large. Note that, for r , if $s_{i,c} < 0$ the gradient is 0, and if $s_{i,c} < s_{j,c}$ the score $s_{i,c}$ will decrease towards 0. This means that if the model predicts that a class is absent, *i.e.* the score is negative, the contours are disregarded. There is no analogous lower score bound for the likelihood l .

Furthermore, since the classes are considered independently, it no longer makes sense to compute the loss over classes that are not present. Their scores should be minimized over the entire image, which is handled by the classification loss. Enforcing prediction contours may only hurt performance, so we mask out these classes and only apply FSL on classes that are present in the image.

Finally, we fix the parameters in FSL to $\mu = 2.5$ and $\sigma = 5$, as opposed to learn them, as this can lead to trivial solutions. For instance, the gradient with respect to μ is always negative, so μ will only increase during training. This might yield inconsistent results in cases where the training time varies, *e.g.* when more gradient steps are performed as a consequence of a larger dataset. To find the optimal parameter values, we optimize \mathcal{L}_{fs} over initial Gaussian CAMs, and compare the region similarity and contour quality. In the spirit of the weakly supervised setting, we only use one image per class, in order to reduce the required ground-truth masks for computing the metrics. For further details, see the supplementary material.

5. Experiments

5.1. Implementation details

Datasets. We test our approach on two datasets; *PASCAL Visual Object Classes* (VOC) [12], and the larger *MS Common Objects in Context* (COCO) [32]. VOC contains 1,464 training images, 1,449 validation images, 1,456 hold-out test images, and includes 20 foreground classes. Following the common practice, we include additional training data from SBD [16], increasing the number of training images to 10,582. For COCO, we use the 2014 train-validation split, which contains 82,783 training images, 40,504 validation images, and includes 80 classes. Note that, although pixel-level segmentation ground truth is available for the training and validation sets, they are not used for training.

Evaluation metrics. For evaluation, we use two complementary metrics as in [19]. (1) Region similarity, \mathcal{J} , which is commonly used in WSSS. It compares segmentation masks in terms of the Jaccard index [18], or the mean

intersection over union (mIoU). (2) We complement this by also evaluating the contour quality, \mathcal{F} , drawing inspiration from the well-established DAVIS benchmark for video object segmentation [37]. This is the F-score computed on the segmentation mask contours, which is efficiently approximated using morphological operations to accumulate bipartite matches of the boundaries between the predicted and ground-truth masks. Finally, we compute a combined metric, $\mathcal{J}\&\mathcal{F}$, which is simply an average of \mathcal{J} and \mathcal{F} .

Training details. Since we apply ISL and FSL to a wide variety of SOTA baselines, we mainly use the default settings and parameters stated in the respective papers or linked code repositories. Moreover, we use the implementations referenced to in the papers, as is. Any deviations from the default settings are listed in the subsequent paragraphs. Note that we did not manage to reproduce the reported results exactly in all cases. Potential reasons include different software and hardware configurations, and the use of different evaluation code. We believe the most likely reason is that the training is spread out over multiple code repositories, where the first stage is typically maintained by the authors, and the final training code is maintained by someone else. For a further discussion, see the supplementary material. Still, our experiments provide good comparisons as they show how ISL and FSL can boost the performance under the same conditions as the baselines, and as the reproduced results are close to the reported results in the literature. We used four A100 40GB GPUs in our experiments.

SEAM [46]. We set the background parameter to 1 and 24 (originally 4 and 24) for AffinityNet, when using ISL. On COCO, FSL was scaled down by a factor of 0.2, and the number of training steps was increased from 20k to 200k for the segmentation network due to the larger dataset size.

SIPE [7]. ISL and FSL were scaled down by a factor of 0.1, since SIPE uses a higher learning rate by default. For FSL, we upsample the CAMs by a factor of 2 (from 32×32 to 64×64), to be closer to SEAM (56×56). We chose an integer factor to avoid artifacts. Note that the ResNet-101 implementation for VOC referenced by SIPE [7] uses COCO pretrained weights, which means that ground-truth segmentation masks were used, and thus, these reproduced results are not weakly supervised strictly speaking.

PMM [30]. We use ISL only during multi-scale training, and FSL during both multi-scale and multi-crop training.

MCTformer [51]. ISL and FSL were scaled down by a factor of 0.1, since MCTformer uses the AdamW optimizer [33] instead of SGD. For FSL, we upsample the CAMs by a factor of 4 (from 14×14 to 56×56) to match SEAM.

Spatial-BCE [49]. Same as the original setting, the foreground and background pixel thresholds in IRN [1] were set to 0.60 and 0.25 respectively. The semantic segmentation threshold was set to 0.30 with ISL, and 0.40 with FSL.

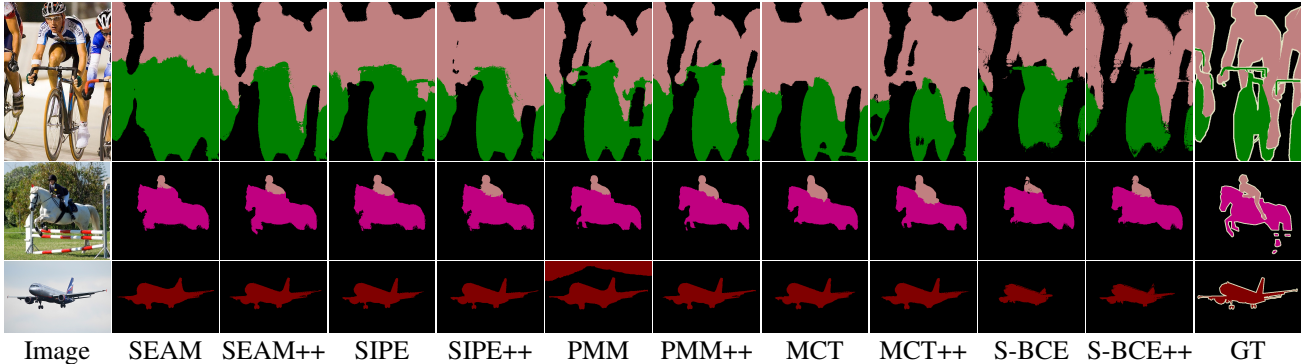


Figure 5: Qualitative results for the implemented methods. “++” indicates that ISL and FSL are used.

Table 1: Region similarity (\mathcal{J}), contour quality (\mathcal{F}), and averaged ($\mathcal{J}\&\mathcal{F}$) on the VOC training set when varying the number of sampled pixels, with $\lambda = 1$ and without FSL.

#pixels	\mathcal{J}	\mathcal{F}	$\mathcal{J}\&\mathcal{F}$
1	61.6 \pm 0.8	40.4 \pm 0.6	51.0 \pm 0.7
5	62.6 \pm 0.6	40.7 \pm 0.6	51.6 \pm 0.6
10	63.0 \pm 0.4	41.2 \pm 0.4	52.1 \pm 0.4
50	63.0 \pm 0.6	41.3 \pm 0.7	52.1 \pm 0.6
100	62.9 \pm 0.7	41.2 \pm 0.7	52.0 \pm 0.7

5.2. Ablation study

We use SEAM [46] as a baseline in the following ablations. Mean and standard deviation is reported over five runs whenever confidence intervals are given.

Number of sampled pixels for ISL. In Table 1 we show the region similarity and contour quality when varying the number of sampled pixels during importance sampling. We observe a boost in performance when increasing the number of samples up to 10. Beyond that, we see little to no improvement. Thus, we fix the number of samples to 10, in order to keep the computational cost as low as possible while maintaining a high segmentation performance.

Optimal loss weight λ for ISL. In Figure 6 we show the segmentation performance when varying the loss weight λ between GAP and ISL in (16). The highest combined score $\mathcal{J}\&\mathcal{F}$ is achieved for $\lambda = 0.2$ both with and without FSL. Importance sampling has a larger impact on the contour quality which is increased by +2.8 and +1.7 points with and without FSL respectively, for $\lambda = 0.2$. The region similarity is less affected by importance sampling, slightly increasing without FSL, and slightly decreasing with it. For a good balance, we fix $\lambda = 0.2$ for subsequent experiments.

Gating function in FSL. We compared $g(r_i, r_j)$ and $g(l_i, l_j)$ based on ReLU with max normalization for r in (4), and the likelihood estimate l in (14), respectively. The normalized CAM, r , performed better with $\mathcal{J}=66.9$ (cf. 64.6),

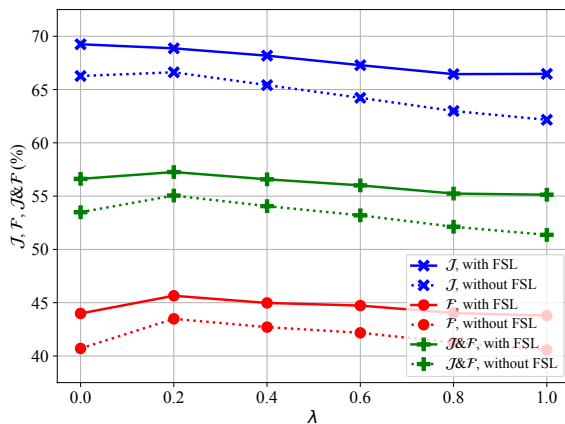


Figure 6: Region similarity (\mathcal{J}), contour quality (\mathcal{F}) and combined ($\mathcal{J}\&\mathcal{F}$) on the VOC training set, as functions of the loss parameter λ , with and without feature similarity loss (FSL). FSL parameters are set to $\mu = 2.5$ and $\sigma = 5$.

$\mathcal{F}=43.5$ (cf. 43.0), and $\mathcal{J}\&\mathcal{F}=55.2$ (cf. 53.8). The reason for worse performance for l could be that the gradient is suppressed too much, as the gradient is upper bounded by $\exp(-x)$, which diminishes faster than $1/x$ for r . See Section 4.2. Also note that there is no lower bound for how far down the scores can be pushed for l , which there is for r .

Likelihood versus posterior. To isolate the effect of modeling the likelihood versus the multinomial posterior, we evaluate the baseline method SEAM using both, and apply ISL and FSL separately. The segmentation performance is displayed in Table 2. Both models are trained with their respective optimal values for λ , which are 0.2 for the likelihood, and 0.6 for the posterior, when used with GAP. The background parameter α , for amplifying and weakening the class scores during CRF for AffinityNet, are also chosen to suit the respective models. 1 and 24 are used for the likelihood, and 2 and 4 for the posterior. With ISL, modeling the likelihood improves the region similarity by +1.3 points over the posterior, and the contour quality is improved by

Table 2: Comparison between modeling the posterior in (5) versus the likelihood in (14) for ISL and FSL, with SEAM [46]. The region similarity (\mathcal{J}), contour quality (\mathcal{F}), and averaged ($\mathcal{J}\&\mathcal{F}$) are computed on the VOC validation set.

Loss	Model	\mathcal{J}	\mathcal{F}	$\mathcal{J}\&\mathcal{F}$
ISL	Posterior	63.0 \pm 0.5	41.0 \pm 0.4	52.0 \pm 0.4
	Likelihood	64.3 \pm 0.8	42.2 \pm 0.6	53.3 \pm 0.7
FSL	Posterior	50.3 \pm 1.3	41.4 \pm 8.5	45.9 \pm 1.1
	Likelihood	66.9 \pm 0.4	43.5 \pm 0.2	55.2 \pm 0.2

Table 3: Region similarity (\mathcal{J}), contour quality (\mathcal{F}), and combined ($\mathcal{J}\&\mathcal{F}$) on the COCO validation set. The classification networks were trained for 8 epochs (three runs) and 16 epochs (single run with fixed seed).

Method	Epochs	\mathcal{J}	\mathcal{F}	$\mathcal{J}\&\mathcal{F}$
SEAM [46]	8	35.9 \pm 0.2	28.2 \pm 0.3	32.1 \pm 0.3
SEAM++ (ours)	8	36.8 \pm 0.2	28.9 \pm 0.1	32.8 \pm 0.1
SEAM [46]	16	35.5	28.5	32.0
SEAM++ (ours)	16	37.8	29.1	33.4

+1.2 points. With FSL, training becomes unstable when it is applied to the posterior. We observed a big variance over five runs, with the region similarity ranging from 40 to 61. However, it is worth noting that for successful runs, the contour quality reached as far as 48. But on average, modeling the posterior underperformed the likelihood. Note that, not only is the performance improved with the likelihood. A further benefit is that it allows ISL and FSL to be applied seamlessly to essentially any method.

5.3. VOC comparison on different SOTA baselines

To evaluate our proposed techniques, we apply them to a wide variety of state-of-the-art baselines. Table 4 shows the reproduced segmentation performance on the VOC validation set for the original methods, as well as when trained with ISL and FSL. A general trend is that ISL mainly improves the contour quality, \mathcal{F} , increasing it by +1.0 points on average without FSL, and +0.7 with it. ISL improves the region similarity, \mathcal{J} , by +0.3, both with and without FSL. The feature similarity loss significantly improves both metrics. \mathcal{J} is increased by +1.1, whether or not ISL is used, and \mathcal{F} is improved by +1.8 without ISL, and by +1.6 with it. With both ISL and FSL, \mathcal{J} , \mathcal{F} and $\mathcal{J}\&\mathcal{F}$ are improved by +1.5, +2.5 and +2.0 points respectively. Note that we even manage to boost the performance of a transformer-based method, MCTformer [51], despite its low CAM resolution of 14×14 , and architectural differences to the CNN-based methods. For qualitative results see Figure 5.

We also evaluate the methods on the test set, improving

Table 4: Region similarity (\mathcal{J}), contour quality (\mathcal{F}), and combined ($\mathcal{J}\&\mathcal{F}$) on the VOC validation set, comparing ISL and FSL on different state-of-the-art baselines.

Method	Backb.	ISL	FSL	\mathcal{J}	\mathcal{F}	$\mathcal{J}\&\mathcal{F}$
SEAM [46]	Res38			63.9 \pm 0.5	39.9 \pm 0.2	51.9 \pm 0.3
	Res38	✓		64.3 \pm 0.8	42.2 \pm 0.6	53.3 \pm 0.7
	Res38		✓	66.9 \pm 0.4	43.5 \pm 0.2	55.2 \pm 0.2
	Res38	✓	✓	66.7 \pm 0.2	44.7 \pm 0.1	55.7 \pm 0.1
Final improvement:				+2.8	+4.8	+3.8
SIPE [7]	Res38			68.0 \pm 0.2	45.1 \pm 0.2	56.6 \pm 0.1
	Res38	✓		68.1 \pm 0.4	46.2 \pm 0.2	57.1 \pm 0.2
	Res38		✓	68.4 \pm 0.3	46.3 \pm 0.2	57.4 \pm 0.2
	Res38	✓	✓	68.3 \pm 0.2	46.8 \pm 0.2	57.6 \pm 0.1
Final improvement:				+0.3	+1.7	+1.0
SIPE [7]	Res101			68.5 \pm 0.2	41.9 \pm 0.5	55.2 \pm 0.3
	Res101	✓		69.2 \pm 0.2	43.3 \pm 0.3	56.3 \pm 0.3
	Res101		✓	68.9 \pm 0.2	43.0 \pm 0.2	56.0 \pm 0.2
	Res101	✓	✓	69.4 \pm 0.2	43.9 \pm 0.2	56.7 \pm 0.1
Final improvement:				+0.9	+2.0	+1.5
PMM [30]	Res38			64.7 \pm 0.5	44.5 \pm 0.5	54.6 \pm 0.4
	Res38	✓		65.0 \pm 1.0	44.6 \pm 0.5	54.8 \pm 0.5
	Res38		✓	66.0 \pm 0.3	46.0 \pm 0.5	56.0 \pm 0.4
	Res38	✓	✓	66.7 \pm 0.7	46.3 \pm 0.6	56.5 \pm 0.6
Final improvement:				+2.0	+1.8	+1.9
MCTformer [51]	DeiT-S			67.5 \pm 1.7	46.7 \pm 0.7	57.1 \pm 1.2
	DeiT-S	✓		67.5 \pm 1.4	47.1 \pm 0.9	57.3 \pm 1.1
	DeiT-S		✓	68.5 \pm 1.2	47.0 \pm 0.5	57.8 \pm 0.9
	DeiT-S	✓	✓	68.3 \pm 0.7	47.3 \pm 0.3	57.8 \pm 0.5
Final improvement:				+0.8	+0.6	+0.7
Spatial-BCE [49]	Res38			68.1 \pm 0.1	45.4 \pm 0.1	56.7 \pm 0.1
	Res38	✓		68.2 \pm 0.2	46.2 \pm 0.1	57.2 \pm 0.1
	Res38		✓	68.8 \pm 0.1	47.6 \pm 0.1	58.2 \pm 0.1
	Res38	✓	✓	69.3 \pm 0.2	48.2 \pm 0.1	58.8 \pm 0.1
Final improvement:				+1.2	+2.8	+2.1
Spatial-BCE [49]	Res101			67.9 \pm 0.2	46.1 \pm 0.1	57.0 \pm 0.1
	Res101	✓		68.5 \pm 0.2	47.8 \pm 0.2	58.1 \pm 0.1
	Res101		✓	69.0 \pm 0.2	48.9 \pm 0.2	59.0 \pm 0.2
	Res101	✓	✓	70.1 \pm 0.2	50.5 \pm 0.2	60.3 \pm 0.2
Final improvement:				+2.2	+4.4	+3.3

\mathcal{J} for SEAM [46] and SIPE [7] by +1.9 and +0.6 points respectively, compared to the literature. Since we did not manage to reproduce the other methods fully, their test scores were not improved. Since we are mainly interested in the combined score, $\mathcal{J}\&\mathcal{F}$, which is not available on the test set, we refer the reader to the supplementary material for full details and the limits of reproducibility.

5.4. Comparison on COCO

We evaluate our proposed method in Table 3 on the large-scale COCO dataset, which contains roughly 10 times more images than VOC. On SEAM [46], we manage to boost the

segmentation performance in this setting as well. When training the classification network for 8 epochs, we boost \mathcal{J} , \mathcal{F} , and $\mathcal{J}\&\mathcal{F}$ by +0.9, +0.7, and +0.7 points respectively. Our method further benefits from longer training, increasing the results by an additional +1.0, +0.2, and +0.6 points, while SEAM is less affected by the longer training.

6. Conclusions

In this work, we improve two previous techniques, importance sampling, and feature similarity loss, for weakly-supervised segmentation. Based on the argument that object classes are not mutually exclusive within image regions, we model the likelihood as opposed to the multinomial posterior, which results in an add-on method that can boost the segmentation performance. This is demonstrated on several state-of-the-art baselines on the VOC and COCO datasets.

Acknowledgments

This work was partially supported by the Wallenberg AI, Autonomous Systems and Software Program (WASP), funded by the Knut and Alice Wallenberg (KAW) Foundation. The computational resources were provided by the National Academic Infrastructure for Supercomputing in Sweden (NAISS), partially funded by the Swedish Research Council through grant agreement no. 2022-06725, and by the Berzelius resource, provided by the KAW Foundation at the National Supercomputer Centre (NSC).

References

- [1] Jiwoon Ahn, Sunghyun Cho, and Suha Kwak. Weakly supervised learning of instance segmentation with inter-pixel relations. In *Proceedings of the IEEE/CVF Conference on Computer Vision and Pattern Recognition*, pages 2209–2218, 2019.
- [2] Jiwoon Ahn and Suha Kwak. Learning pixel-level semantic affinity with image-level supervision for weakly supervised semantic segmentation. In *Proceedings of the IEEE Conference on Computer Vision and Pattern Recognition*, pages 4981–4990, 2018.
- [3] Nikita Araslanov and Stefan Roth. Single-stage semantic segmentation from image labels. In *Proceedings of the IEEE/CVF Conference on Computer Vision and Pattern Recognition (CVPR)*, June 2020.
- [4] Amy Bearman, Olga Russakovsky, Vittorio Ferrari, and Li Fei-Fei. What’s the point: Semantic segmentation with point supervision. In *Computer Vision–ECCV 2016: 14th European Conference, Amsterdam, The Netherlands, October 11–14, 2016, Proceedings, Part VII 14*, pages 549–565. Springer, 2016.
- [5] Amy Bearman, Olga Russakovsky, Vittorio Ferrari, and Li Fei-Fei. What’s the point: Semantic segmentation with point supervision. In *European Conference on Computer Vision*, pages 549–565. Springer, 2016.
- [6] Liyi Chen, Weiwei Wu, Chenchen Fu, Xiao Han, and Yuntao Zhang. Weakly supervised semantic segmentation with boundary exploration. In *Computer Vision–ECCV 2020: 16th European Conference, Glasgow, UK, August 23–28, 2020, Proceedings, Part XXVI 16*, pages 347–362. Springer, 2020.
- [7] Qi Chen, Lingxiao Yang, Jian-Huang Lai, and Xiaohua Xie. Self-supervised image-specific prototype exploration for weakly supervised semantic segmentation. In *Proceedings of the IEEE/CVF Conference on Computer Vision and Pattern Recognition (CVPR)*, pages 4288–4298, June 2022.
- [8] Zhaozheng Chen, Tan Wang, Xiongwei Wu, Xian-Sheng Hua, Hanwang Zhang, and Qianru Sun. Class re-activation maps for weakly-supervised semantic segmentation. In *Proceedings of the IEEE/CVF Conference on Computer Vision and Pattern Recognition (CVPR)*, pages 969–978, June 2022.
- [9] Marius Cordts, Mohamed Omran, Sebastian Ramos, Timo Rehfeld, Markus Enzweiler, Rodrigo Benenson, Uwe Franke, Stefan Roth, and Bernt Schiele. The cityscapes dataset for semantic urban scene understanding. In *Proceedings of the IEEE conference on computer vision and pattern recognition*, pages 3213–3223, 2016.
- [10] Jifeng Dai, Kaiming He, and Jian Sun. Boxesup: Exploiting bounding boxes to supervise convolutional networks for semantic segmentation. In *Proceedings of the IEEE International Conference on Computer Vision*, pages 1635–1643, 2015.
- [11] Ye Du, Zehua Fu, Qingjie Liu, and Yunhong Wang. Weakly supervised semantic segmentation by pixel-to-prototype contrast. In *Proceedings of the IEEE/CVF Conference on Computer Vision and Pattern Recognition (CVPR)*, pages 4320–4329, June 2022.
- [12] Mark Everingham, Luc Van Gool, Christopher KI Williams, John Winn, and Andrew Zisserman. The pascal visual object classes (voc) challenge. *International Journal of Computer Vision*, 88(2):303–338, 2010.
- [13] Junsong Fan, Zhaoxiang Zhang, Chunfeng Song, and Tieniu Tan. Learning integral objects with intra-class discriminator for weakly-supervised semantic segmentation. In *Proceedings of the IEEE/CVF Conference on Computer Vision and Pattern Recognition*, pages 4283–4292, 2020.
- [14] Junsong Fan, Zhaoxiang Zhang, Tieniu Tan, Chunfeng Song, and Jun Xiao. Cian: Cross-image affinity net for weakly supervised semantic segmentation. In *Proceedings of the AAAI Conference on Artificial Intelligence*, volume 34, pages 10762–10769, 2020.
- [15] Monica Gruosso, Nicola Capece, and Ugo Erra. Human segmentation in surveillance video with deep learning. *Multi-media Tools and Applications*, 80:1175–1199, 2021.
- [16] Bharath Hariharan, Pablo Arbeláez, Lubomir Bourdev, Subhransu Maji, and Jitendra Malik. Semantic contours from inverse detectors. In *2011 International Conference on Computer Vision*, pages 991–998. IEEE, 2011.
- [17] Zilong Huang, Xinggong Wang, Jiasi Wang, Wenyu Liu, and Jingdong Wang. Weakly-supervised semantic segmentation network with deep seeded region growing. In *Proceedings of the IEEE Conference on Computer Vision and Pattern Recognition*, pages 7014–7023, 2018.

- [18] Paul Jaccard. Distribution de la flore alpine dans le bassin des dranses et dans quelques régions voisines. *Bulletin de la Société Vaudoise des Sciences Naturelles*, 37:241–272, 1901.
- [19] Arvi Jonnarth and Michael Felsberg. Importance sampling CAMs for weakly-supervised segmentation. In *IEEE International Conference on Acoustics, Speech, and Signal Processing (ICASSP)*, pages 2639–2643, 2022.
- [20] Anna Khoreva, Rodrigo Benenson, Jan Hosang, Matthias Hein, and Bernt Schiele. Simple does it: Weakly supervised instance and semantic segmentation. In *Proceedings of the IEEE Conference on Computer Vision and Pattern Recognition*, pages 876–885, 2017.
- [21] Alexander Kolesnikov and Christoph H Lampert. Seed, expand and constrain: Three principles for weakly-supervised image segmentation. In *European Conference on Computer Vision*, pages 695–711. Springer, 2016.
- [22] Philipp Krähenbühl and Vladlen Koltun. Efficient inference in fully connected crfs with gaussian edge potentials. *Advances in Neural Information Processing Systems*, 24:109–117, 2011.
- [23] Hyeokjun Kweon, Sung-Hoon Yoon, Hyeonseong Kim, Daehee Park, and Kuk-Jin Yoon. Unlocking the potential of ordinary classifier: Class-specific adversarial erasing framework for weakly supervised semantic segmentation. In *Proceedings of the IEEE/CVF International Conference on Computer Vision (ICCV)*, pages 6994–7003, October 2021.
- [24] Jungbeom Lee, Jooyoung Choi, Jisoo Mok, and Sungroh Yoon. Reducing information bottleneck for weakly supervised semantic segmentation. *Advances in Neural Information Processing Systems*, 34, 2021.
- [25] Jungbeom Lee, Eunji Kim, Sungmin Lee, Jangho Lee, and Sungroh Yoon. Ficklenet: Weakly and semi-supervised semantic image segmentation using stochastic inference. In *Proceedings of the IEEE/CVF Conference on Computer Vision and Pattern Recognition*, pages 5267–5276, 2019.
- [26] Jungbeom Lee, Eunji Kim, and Sungroh Yoon. Anti-adversarially manipulated attributions for weakly and semi-supervised semantic segmentation. In *Proceedings of the IEEE/CVF Conference on Computer Vision and Pattern Recognition*, pages 4071–4080, 2021.
- [27] Jungbeom Lee, Jihun Yi, Chaehun Shin, and Sungroh Yoon. Bbam: Bounding box attribution map for weakly supervised semantic and instance segmentation. In *Proceedings of the IEEE/CVF conference on computer vision and pattern recognition*, pages 2643–2652, 2021.
- [28] Jing Li, Junsong Fan, and Zhaoxiang Zhang. Towards noiseless object contours for weakly supervised semantic segmentation. In *Proceedings of the IEEE/CVF Conference on Computer Vision and Pattern Recognition (CVPR)*, pages 16856–16865, June 2022.
- [29] Kunpeng Li, Ziyang Wu, Kuan-Chuan Peng, Jan Ernst, and Yun Fu. Tell me where to look: Guided attention inference network. In *Proceedings of the IEEE conference on computer vision and pattern recognition*, pages 9215–9223, 2018.
- [30] Yi Li, Zhanghui Kuang, Liyang Liu, Yimin Chen, and Wayne Zhang. Pseudo-mask matters in weakly-supervised semantic segmentation. In *Proceedings of the IEEE/CVF International Conference on Computer Vision (ICCV)*, pages 6964–6973, October 2021.
- [31] Di Lin, Jifeng Dai, Jiaya Jia, Kaiming He, and Jian Sun. Scribblesup: Scribble-supervised convolutional networks for semantic segmentation. In *Proceedings of the IEEE conference on computer vision and pattern recognition*, pages 3159–3167, 2016.
- [32] Tsung-Yi Lin, Michael Maire, Serge Belongie, James Hays, Pietro Perona, Deva Ramanan, Piotr Dollár, and C Lawrence Zitnick. Microsoft coco: Common objects in context. In *European Conference on Computer Vision*, pages 740–755. Springer, 2014.
- [33] Ilya Loshchilov and Frank Hutter. Decoupled weight decay regularization. In *International Conference on Learning Representations*, 2019.
- [34] Shervin Minaee, Yuri Y Boykov, Fatih Porikli, Antonio J Plaza, Nasser Kehtarnavaz, and Demetri Terzopoulos. Image segmentation using deep learning: A survey. *IEEE transactions on pattern analysis and machine intelligence*, 2021.
- [35] George Papandreou, Liang-Chieh Chen, Kevin P Murphy, and Alan L Yuille. Weakly- and semi-supervised learning of a deep convolutional network for semantic image segmentation. In *Proceedings of the IEEE International Conference on Computer Vision*, pages 1742–1750, 2015.
- [36] Deepak Pathak, Philipp Krähenbühl, and Trevor Darrell. Constrained convolutional neural networks for weakly supervised segmentation. In *Proceedings of the IEEE International Conference on Computer Vision*, pages 1796–1804, 2015.
- [37] Federico Perazzi, Jordi Pont-Tuset, Brian McWilliams, Luc Van Gool, Markus Gross, and Alexander Sorkine-Hornung. A benchmark dataset and evaluation methodology for video object segmentation. In *Proceedings of the IEEE Conference on Computer Vision and Pattern Recognition*, pages 724–732, 2016.
- [38] Xiaojuan Qi, Zhengzhe Liu, Jianping Shi, Hengshuang Zhao, and Jiaya Jia. Augmented feedback in semantic segmentation under image level supervision. In *European Conference on Computer Vision*, pages 90–105. Springer, 2016.
- [39] Simone Rossetti, Damiano Zappia, Marta Sanzari, Marco Schaerf, and Fiorenza Pirri. Max pooling with vision transformers reconciles class and shape in weakly supervised semantic segmentation. In *Computer Vision—ECCV 2022: 17th European Conference, Tel Aviv, Israel, October 23–27, 2022, Proceedings, Part XXX*, pages 446–463. Springer, 2022.
- [40] Lixiang Ru, Yibing Zhan, Baosheng Yu, and Bo Du. Learning affinity from attention: End-to-end weakly-supervised semantic segmentation with transformers. In *Proceedings of the IEEE/CVF Conference on Computer Vision and Pattern Recognition (CVPR)*, pages 16846–16855, June 2022.
- [41] Wataru Shimoda and Keiji Yanai. Self-supervised difference detection for weakly-supervised semantic segmentation. In *Proceedings of the IEEE/CVF International Conference on Computer Vision*, pages 5208–5217, 2019.
- [42] Yukun Su, Ruizhou Sun, Guosheng Lin, and Qingyao Wu. Context decoupling augmentation for weakly supervised se-

- semantic segmentation. In *Proceedings of the IEEE/CVF International Conference on Computer Vision (ICCV)*, pages 7004–7014, October 2021.
- [43] Guolei Sun, Wenguan Wang, Jifeng Dai, and Luc Van Gool. Mining cross-image semantics for weakly supervised semantic segmentation. In *European conference on computer vision*, pages 347–365. Springer, 2020.
- [44] Kunyang Sun, Haoqing Shi, Zhengming Zhang, and Yongming Huang. Ecs-net: Improving weakly supervised semantic segmentation by using connections between class activation maps. In *Proceedings of the IEEE/CVF International Conference on Computer Vision (ICCV)*, pages 7283–7292, October 2021.
- [45] Paul Vernaza and Manmohan Chandraker. Learning random-walk label propagation for weakly-supervised semantic segmentation. In *Proceedings of the IEEE Conference on Computer Vision and Pattern Recognition*, pages 7158–7166, 2017.
- [46] Yude Wang, Jie Zhang, Meina Kan, Shiguang Shan, and Xilin Chen. Self-supervised equivariant attention mechanism for weakly supervised semantic segmentation. In *Proceedings of the IEEE/CVF Conference on Computer Vision and Pattern Recognition*, pages 12275–12284, 2020.
- [47] Yunchao Wei, Jiashi Feng, Xiaodan Liang, Ming-Ming Cheng, Yao Zhao, and Shuicheng Yan. Object region mining with adversarial erasing: A simple classification to semantic segmentation approach. In *Proceedings of the IEEE conference on computer vision and pattern recognition*, pages 1568–1576, 2017.
- [48] Yunchao Wei, Huaxin Xiao, Honghui Shi, Zequn Jie, Jiashi Feng, and Thomas S Huang. Revisiting dilated convolution: A simple approach for weakly- and semi-supervised semantic segmentation. In *Proceedings of the IEEE Conference on Computer Vision and Pattern Recognition*, pages 7268–7277, 2018.
- [49] Tong Wu, Guangyu Gao, Junshi Huang, Xiaolin Wei, Xiaoming Wei, and Chi Harold Liu. Adaptive spatial-bce loss for weakly supervised semantic segmentation. In *Computer Vision—ECCV 2022: 17th European Conference, Tel Aviv, Israel, October 23–27, 2022, Proceedings, Part XXIX*, pages 199–216. Springer, 2022.
- [50] Tong Wu, Junshi Huang, Guangyu Gao, Xiaoming Wei, Xiaolin Wei, Xuan Luo, and Chi Harold Liu. Embedded discriminative attention mechanism for weakly supervised semantic segmentation. In *Proceedings of the IEEE/CVF Conference on Computer Vision and Pattern Recognition*, pages 16765–16774, 2021.
- [51] Lian Xu, Wanli Ouyang, Mohammed Bennamoun, Farid Boussaid, and Dan Xu. Multi-class token transformer for weakly supervised semantic segmentation. In *Proceedings of the IEEE/CVF Conference on Computer Vision and Pattern Recognition (CVPR)*, pages 4310–4319, June 2022.
- [52] Sung-Hoon Yoon, Hyeokjun Kweon, Jegyeong Cho, Shinjeong Kim, and Kuk-Jin Yoon. Adversarial erasing framework via triplet with gated pyramid pooling layer for weakly supervised semantic segmentation. In *Computer Vision—ECCV 2022: 17th European Conference, Tel Aviv, Israel, October 23–27, 2022, Proceedings, Part XXIX*, pages 326–344. Springer, 2022.
- [53] Dong Zhang, Hanwang Zhang, Jinhui Tang, Xian-Sheng Hua, and Qianru Sun. Causal intervention for weakly-supervised semantic segmentation. In H. Larochelle, M. Ranzato, R. Hadsell, M. F. Balcan, and H. Lin, editors, *Advances in Neural Information Processing Systems*, volume 33, pages 655–666. Curran Associates, Inc., 2020.
- [54] Fei Zhang, Chaochen Gu, Chenyue Zhang, and Yuchao Dai. Complementary patch for weakly supervised semantic segmentation. In *Proceedings of the IEEE/CVF International Conference on Computer Vision*, pages 7242–7251, 2021.
- [55] Bolei Zhou, Aditya Khosla, Agata Lapedriza, Aude Oliva, and Antonio Torralba. Learning deep features for discriminative localization. In *Proceedings of the IEEE Conference on Computer Vision and Pattern Recognition*, pages 2921–2929, 2016.

Supplementary Material

This supplementary material contains three parts. (1) The ablation study on how we find the optimal values for the parameters μ and σ in FSL in Section S.1. (2) A state-of-the-art comparison on the VOC validation and test sets in Section S.2. (3) A discussion on reproducibility in weakly-supervised semantic segmentation in Section S.3.

S.1. Ablation study for μ and σ in FSL

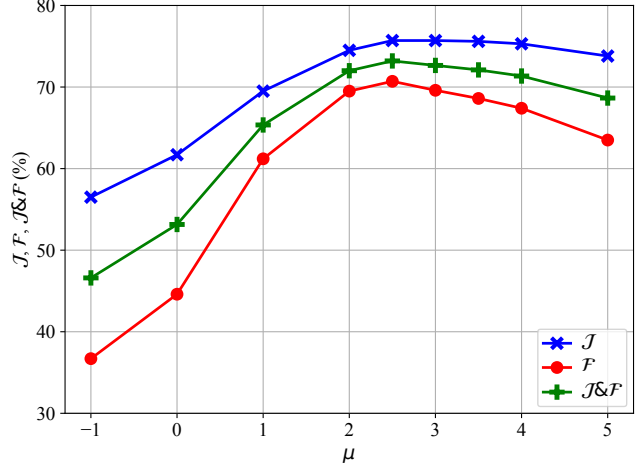
The spatial extent of the feature similarity loss (FSL) is controlled by σ , while the dissimilarity threshold between pixel values is controlled by μ . Since learning them together with the network parameters could lead to trivial solutions, we set them as fixed parameters and find optimal values based on the segmentation performance. In the spirit of the weakly supervised setting, we only use a handful of images, to reduce the required ground-truth masks, and randomly sample one image per class from the VOC training set. Subsequently, we optimize FSL with respect to initial CAMs, and compute the resulting region similarity, \mathcal{J} , and contour quality, \mathcal{F} . Note that no network was involved at this stage.

Due to both simplicity, and to mimic realistic CAMs, we hand-craft initial CAMs for each image, based on the Gaussian function. See Figure 2 in the main paper to get an idea of what the initial CAMs look like. For the unimodal Gaussian CAMs to make sense, we only sampled images that contain a single object. The Gaussian CAMs were defined by the mean and standard deviation of the ground-truth segmentation masks. The mean was computed as the average position of all foreground pixels, and the two non-zero components of the linearly independent diagonal covariance matrix were computed as the variance in the two spatial coordinates. Finally, the non-normalized scores, or logits, were computed as

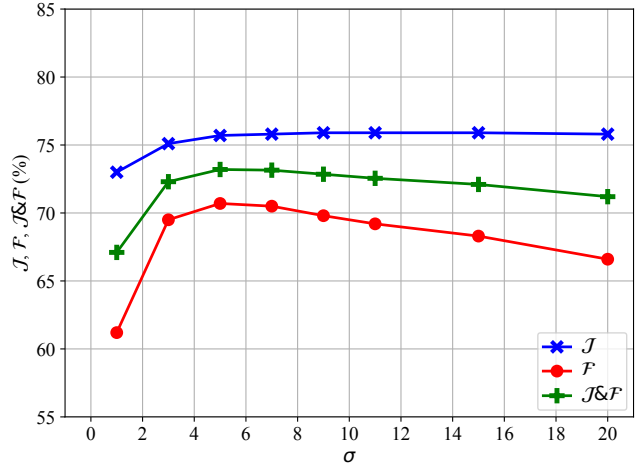
$$s(i, j) = 2G(i, j) - 1, \quad (24)$$

where $G(i, j)$ is the Gaussian function at spatial location (i, j) . This was done to attain negative values outside the object boundaries. Note that, since we only used images with a single object, s contains a single channel, and essentially predicts foreground versus background. The predicted foreground segmentation mask was attained by thresholding the score at zero, where positive values were predicted as foreground.

The segmentation performance after optimizing FSL for different values of μ and σ are shown in Figure 7. The



(a) $\sigma = 5.0$



(b) $\mu = 2.5$

Figure 7: Region similarity (\mathcal{J}), contour quality (\mathcal{F}), and averaged ($\mathcal{J}\&\mathcal{F}$), as functions of (a) μ , and (b) σ , when optimizing Gaussian CAMs on one image per class.

highest combined score $\mathcal{J}\&\mathcal{F}$ is achieved for $\mu = 2.5$ and $\sigma = 5$, so we fix the parameters to these values.

A Gaussian spatial weight with $\sigma = 5$ means that $\sim 39\%$ of the loss contribution comes from pixel pairs that are within 5 pixels apart, while pairs that are within 10 pixels contribute to $\sim 86\%$ of the loss. Note that the CAM resolution is 56×56 when using the ResNet-38 backbone with an

input size of 448×448 , which is the case for our SEAM [46] baseline. Thus, the FSL optimization procedure described above was done in a tenth of the original image resolution, to roughly match the CAM resolution.

A dissimilarity threshold of $\mu = 2.5$ means that pixels are considered similar if their normalized L1 distance δ between the RGB color values in (13) is less than 0.076, since this corresponds to a negative pixel dissimilarity score, *i.e.* $f(\delta) < 0$ in (12).

S.2. VOC test set evaluation

In Table 5 we show the region similarity on the VOC validation and test sets for the implemented methods. We also include reported results for other methods that we did not implement. However, methods that use additional supervision, either directly using other datasets, or indirectly using saliency maps, are excluded. For transparency and completeness, we show both the reported and reproduced results of our implemented methods. The reported results are taken directly from the respective publications. Our reproduced results on the validation set are computed as the average over five runs. For the test set, we submit the segmentation predictions from the best out of the five runs, based on validation \mathcal{J} , to the PASCAL VOC evaluation server.

Compared to the reported results, we improve \mathcal{J} for SEAM [46], and SIPE [7] using ResNet-101, by +1.9 and +0.6 respectively. Since we did not manage to reproduce the other methods fully, their test scores were not improved compared to the reported results. See Section S.3 for potential reasons for this.

However, comparing our reproduced results, with our ISL and FSL, we improve the test \mathcal{J} by +1.1 on average.

The original MCTformer [51] had a larger standard deviation of 1.7 on the validation set, compared to when ISL and FSL were used, which was 0.7. See Table 4 in the main paper. This resulted in that the performance of the best out of five runs for the original method was slightly higher than the best run using ISL and FSL. This explains why our reproduced results on the test set was higher for the original method, and that we observe the opposite case over five runs on the validation set. This observation is important for practitioners who simply apply an off-the-shelf training method. If the training is only run once, a lower variance is beneficial, as the performance deviation is smaller, and the resulting model is more likely to perform as expected.

S.3. Discussion on the limits of reproducibility

As stated in the main paper, we use the implementations referenced to in the respective publications, as is, with only minor modifications described in Section 5.1. Still, we did not manage to reproduce the reported results exactly, in all cases. We believe that weakly-supervised segmentation is especially tricky from a reproducibility perspective,

Table 5: Region similarity comparison on the VOC validation and test sets, including both reported values in the respective publications and our reproduced results. “++” denotes the improved methods using our ISL and FSL.

Method	Backb.	Reported		Reproduced	
		val	test	val	test
CCNN [36]	VGG16	35.3	35.6	-	-
EM-Adapt [35]	VGG16	38.2	39.6	-	-
SEC [21]	VGG16	50.7	51.7	-	-
AugFeed [38]	VGG16	54.3	55.5	-	-
AffinityNet [2]	Res38	61.7	63.7	-	-
ICD [13]	Res101	64.1	64.3	-	-
CIAN [14]	Res101	64.3	65.3	-	-
SSDD [41]	Res38	64.9	65.5	-	-
AFA [40]	MiT-B1	66.0	66.3	-	-
CONTA [53]	Res38	66.1	66.7	-	-
CDA [42]	Res38	66.1	66.8	-	-
MCIS [43]	Res101	66.2	66.9	-	-
PPC [11]	Res38	67.7	67.4	-	-
ECS-Net [44]	Res38	66.6	67.6	-	-
CGNet [23]	Res38	68.4	68.2	-	-
ReCAM [8]	Res101	68.5	68.4	-	-
CPN [54]	Res38	67.8	68.5	-	-
RIB [24]	Res101	68.3	68.6	-	-
ViT-PCM [39]	ViT-B	70.3	70.9	-	-
AEFT [52]	Res38	70.9	71.7	-	-
SANCE [28]	Res101	70.9	72.2	-	-
SEAM [46]	Res38	64.5	65.7	63.9	65.4
SEAM++	Res38	-	-	66.7	67.6
SIPE [7]	Res38	68.2	69.5	68.0	68.9
SIPE++	Res38	-	-	68.3	69.4
SIPE [7]	Res101	68.8	69.7	68.5	69.4
SIPE++	Res101	-	-	69.4	70.3
PMM [30]	Res38	68.5	69.0	64.7	65.7
PMM++	Res38	-	-	66.7	67.0
MCTformer [51]	DeiT-S	71.9	71.6	67.5	70.6
MCTformer++	DeiT-S	-	-	68.3	70.0
Spatial-BCE [49]	Res38	70.0	71.3	68.1	68.4
Spatial-BCE++	Res38	-	-	69.3	69.4
Spatial-BCE [49]	Res101	-	-	67.9	68.4
Spatial-BCE++	Res101	-	-	70.1	70.6

as it involves multiple steps to arrive at the final model. In chronological order, these are: (1) Downloading data and pre-trained weights; (2) training a classification network, (3) generating CAMs; (4) optionally generating labels for a pseudo-label refinement method; (5) optionally training

Table 6: List of code repositories used for reproducing the results. See Section S.3 for what each step involves.

Method	Steps	Code repository
SEAM [46]	1-6	https://github.com/YudeWang/SEAM
	7-9	https://github.com/YudeWang/semantic-segmentation-codebase
SIPE [7]	1-6	https://github.com/chenqi1126/SIPE
	7-9 w/ Res38	https://github.com/YudeWang/semantic-segmentation-codebase
	7-9 w/ Res101	https://github.com/kazuto1011/deeplab-pytorch
PMM [30]	1-3, 6	https://github.com/Eli-YiLi/PMM
	7-9	https://github.com/Eli-YiLi/WSSS_MMSeg
MCTformer [51]	1-9	https://github.com/xulianuwa/MCTformer
Spatial-BCE [49]	1-3	https://github.com/allenwu97/Spatial-BCE
	4-6	https://github.com/jiwoon-ahn/irn
	7-9 w/ Res38	https://github.com/YudeWang/semantic-segmentation-codebase
	7-9 w/ Res101	https://github.com/kazuto1011/deeplab-pytorch

or applying a pseudo-label refinement method, *e.g.* IRN [1] or AffinityNet [2]; (6) generating pseudo-labels; (7) training a final segmentation model; (8) optionally applying a post-processing method, *e.g.* CRF [22], and finally; (9) evaluating the final segmentation predictions.

This convoluted pipeline becomes especially tricky to reproduce, due to the fact that the steps are usually split across multiple code repositories. This introduces additional possibilities for misaligned implementation details, especially if they are not fully listed. Commonly, the authors of WSSS papers provide code for steps 1-3, and the subsequent steps are typically implemented in a different code repository, and in some cases even maintained by different authors. See Table 6 for the repositories that we used in the different steps for each method, which includes a total of 9 unique code repositories. A further argument that speaks for this being the main reason, is that we did manage to reproduce the CAM results. The region similarity of our reproduced CAMs matched the reported results within the margin of error, in most cases. See Table 7 for a comparison between reported and reproduced CAM results. In all cases, the CAM results were more closely reproduced than the final segmentation results. This means that the subsequent steps introduce differences in the implementation, which is reasonable as this is typically not the main focus of WSSS papers.

In the case of MCTformer [51], where all stages are contained in a single repository, we still observe a discrepancy between the reported and reproduced results. Moreover, the degree of reproducibility varies between the validation and test results. The gap is by far larger on the validation results, which could possibly be caused by hyperparameter tuning on the validation data, not reflected in the repository. Additionally, this can to some extent be explained by the

Table 7: Region similarity for CAMs without CRF, comparing original results reported in the respective papers in the “Orig.” column, and our reproduced results with max and mean over five runs.

Method	Set	Orig.	Reproduced			
			Original		with ISL/FSL	
			max	mean \pm std	max	mean \pm std
SEAM [46]	<i>train</i>	55.4	55.6	55.0 \pm 0.4	61.0	60.6 \pm 0.3
SIPE [7]	<i>train</i>	58.6	58.7	58.5 \pm 0.2	60.4	60.1 \pm 0.2
PMM [30]	<i>val</i>	56.2	55.4	55.1 \pm 0.2	59.3	58.9 \pm 0.3
MCTformer [51]	<i>train</i>	61.7	61.8	59.4 \pm 2.0	61.6	61.2 \pm 0.4
Spatial-BCE [49]	<i>train</i>	68.1	67.2	67.0 \pm 0.2	68.7	68.6 \pm 0.1

high variance over five runs, where the best run reproduces the reported CAM result in Table 7. If the subsequent steps contain a similar variance, the reported final segmentation result could be achieved as the best out of a larger number of runs.

Furthermore, while most WSSS works carefully state the training details for steps 1-3, it is next to impossible to list the full configuration of the experiments. The following additional items could potentially affect performance:

- Different software configurations, *i.e.* choice of package manager (pip versus conda), python version, python package versions, or CUDA version *etc.*
- Different hardware configurations, *i.e.* number of GPUs, GPU model, CPU model *etc.*
- Different computational environments, *i.e.* OS version, the use of containers *etc.*